Talanta 82 (2010) 620–626

Contents lists available at ScienceDirect

Talanta

journal homepage: www.elsevier.com/locate/talanta

Novel luminescent Ir(III) dyes for developing highly sensitive oxygen sensing films

M. Marin-Suarezdel Toro[a], J.F. Fernandez-Sanchez[a,*], E. Baranoff[b], Md.K. Nazeeruddin[b], M. Graetzel[b], A. Fernandez-Gutierrez[a,*]

[a] Department of Analytical Chemistry, Faculty of Sciences, University of Granada (UGR), C/Fuentenueva s/n, E-18071 Granada, Spain
[b] Sciences and Engineering, Ecole Polytechnique Fédérale de Lausanne (EPFL), CH-1015 Lausanne, Switzerland

ARTICLE INFO

Article history:
Received 4 February 2010
Received in revised form 20 April 2010
Accepted 10 May 2010
Available online 16 May 2010

Keywords:
Luminescence
Sensor
Iridium complex
Oxygen
Nanostructured material

ABSTRACT

New sensing films have been developed for the detection of molecular oxygen. These films are based on luminescent Ir(III) dyes incorporated either into polystyrene (with and without plasticizer) or metal oxide, nanostructured material. The preparation and characterization of each film have been investigated in detail. Due to their high sensitivity for low oxygen concentration, the parameters $p_{O_2}(S = 1/2)$ and $\Delta I_{1\%}$ have been also evaluated in order to establish the most sensitive membrane for controlling concentrations between 0 and 10% and low oxygen concentrations (lower than 1%), respectively. The results show that the use of nanostructured material increased the sensitivity of the film; the most sensitive membrane for controlling O_2 between 0 and 10% is based on N1001 immobilized in AP200/19 ($k_{sv} = 2848 \pm 101$ bar^{-1} and $p_{O_2}(S = 1/2) = 0.0006$), and the complex N969 incorporated into AP200/19 seems to be the most suitable for applications in oxygen trace sensing ($\Delta I_{1\%} = 93.13 \pm 0.13\%$).

1. Introduction

Developing methods for monitoring oxygen concentration in real time has become a priority due to the potential for improved medical diagnostics and management of conditions where oxygen imbalances are manifest [1]; oxygen, often acting as a key metabolite in aerobic systems with a multitude of biological functions, is of major importance in medical applications [2]. In addition, the determination of oxygen is important in other fields such as chemical analysis, packaging, process control, as well as in environmental monitoring [3–6].

Furthermore, oxygen trace sensing has become crucial in microbiology, since a variety of microorganisms grow under special conditions, from atmosphere of residual oxygen to anaerobic conditions [7]. Therefore, oxygen trace sensing has special application in the control of modified atmosphere packaging (MAP) where an adequate oxygen concentration is required inside the package in order to maintain the microbiological stability of fresh-cut fruits and vegetables, by limiting aerobic respiration without inducing anaerobic processes [8]. In addition, oxygen trace control is important for avoiding browning, discoloration and softening, where usually concentration below 0.25–5 kPa of oxygen are needed [9–12]. For keeping the nutritional composition and antioxidant potential of fruits and vegetable, the required oxygen concentration varies from 2 to 10 kPa [10,13].

Optical techniques are attractive for frequent or continuous monitoring because they offer the advantages of high sensitivity and selectivity, insensitivity to electrical interferences, no need for a reference signal and the possibility of remote sensing for "in situ" applications [14]. Optodes are also suitable for high-resolution imaging of solute distributions in complex environments such as aquatic sediments and there are also exciting possibilities for multi-parameter and multi-analyte sensing [15,16]. Thus, optical oxygen sensing has attracted a lot of scientific effort and has received a great deal of attention in recent years as dynamic quenching of the luminescence emission by oxygen has proved to be very sensitive [17].

Numerous probes and polymeric matrices have been reported [18]. Ideally, a matrix must be permeable to oxygen, should be structurally stable enough to withstand the mechanical stress and should increase photostability [19]. In addition, it has to prevent leaching and the migration of chemical compounds by insulation and has to prevent the aggregation of the dye [20–23].

Most of the probes are based on the luminescence quenching of organometallic complexes by paramagnetic oxygen [24–26] immobilized into a solid matrix (Fernandez-Sanchez et al. [17],

* Corresponding authors. Tel.: +34 958248409; fax: +34 958249510.
E-mail addresses: jffernan@ugr.es (J.F. Fernandez-Sanchez), albertof@ugr.es (A. Fernandez-Gutierrez).

0039-9140/$ – see front matter © 2010 Elsevier B.V. All rights reserved.
doi:10.1016/j.talanta.2010.05.018

Table 1
Summary of iridium and ruthenium dyes used as oxygen probes; 2006–2010, update of table in Fernandez-Sanchez et al. [17].

Probe	Support for immobilization	$\lambda_{ex/em}$ (nm)	Φ_L	I_0/I_{100}	Reference
$[Ru(dpp)_2bpy\text{-}OH](PF_6)_2$	Glass*	450/650	–	19	[30]
$[Ru(dpp)_2bpy\text{-}19](PF_6)_2$	Glass	450/625	–	8	[30]
$[Ru(bpy)_2phen]^{2+}$	Mesoporous silica MCM-41*	457/588	–	–	[31]
$[Ru(bpy)_3]^{2+}$	Molecular sieve MSU-3*	–/601	–	–	[32]
$[Ru(dpp)_3]^{2+}$ **	TEOS derived sol-gel matrix	480/590	–	–	[33]
$[Ru(phen)_2(Dppz\text{-}Si)]^{2+}$	ORMOSIL*	480/590	–	3.1	[34]
$[Ru(dpp)_2bpy]^{2+}$	Mesoporous silica MCM-41*	490/610	–	23.2	[29]
$[Ru(bpyPS_2)_3](PF_6)2$	Polystyrene*	450/600	–	–	[35]
$Ir(C_N)_2(acac)$	Polystyrene	477/566	–	–	[28]
$Ir(C_S)_2(acac)$	Polystyrene	455/544	–	–	[28]
$Ir(C_O)_2(acac)$	Polystyrene	472/544	–	–	[28]
$Ir(C_{S\text{-}Me})_2(acac)$	Polystyrene	475/566	–	–	[28]
$(C_S)2Ir(\mu\text{-}Cl)_2Ir(C_S)_2$	Polystyrene	484/588	–	–	[28]
$(C_N)2Ir(\mu\text{-}Cl)_2Ir(C_N)_2$	Polystyrene	463/567	–	–	[28]
N948	Polystyrene	494/665	0.57	–	[19]
	ALOOH	494/665	0.20	–	[19]
L_1H_3	Coordination polymer	385/538	–	–	[36]
L_2H_3	Coordination polymer	400/565	–	–	[36]
$Ir(ppy\text{-}NPh_2)_3$	Ethyl cellulose	405/524	–	–	[37]
$Ir(mebtp)_3$	FIB	296/595	–	7.41	[38]
N969	Polystyrene	385/585	0.86	5.0 ± 0.4	This work
	AlOOH	350/490	0.86	47.6 ± 0.5	This work
N1001	Polystyrene	300/530	0.64	7.3 ± 0.5	This work
	AlOOH	330/549	0.64	4.3 ± 2.3	This work
N1008	Polystyrene	305/510	0.92	8.2 ± 0.7	This work
	AlOOH	340/512	0.92	13.5 ± 1.1	This work
N1010	Polystyrene	300/520	0.14	2.0 ± 0.1	This work
	AlOOH	330/545	0.14	1.2 ± 0.2	This work

* Covalent bound.
** Linked with dendrons.
dpp: 4,7-diphenyl-1,10-phenanthroline; bpy: 2,2′-bipyridine; PF_6: hexafluorophosphate; Dppz-Si: alkoxylane-modified dipyrido[3,2-a:2′,3′-c]phenazine; phen: 1,10-phenanthroline; PS: polystyrene; C_N: 3-(1-methylbenzoimidazol-2-yl)-7-(diethylamino)-coumarin; C_S: 3-(benzothiazol-2-yl)-7-(diethylamino)-coumarin; C_O: 3-(5-chlorobenzooxazol-2-yl)-7-(diethylamino)-coumarin; $C_{S\text{-}Me}$: 3-(benzothiazol-2-yl)-7-(dimethylamino)-coumarin; acac: acetylacetone; N948: Ir(2-phenylpyridine)2(4,4-bis(2-(4-N,Nmethylhexylaminophenyl)ethyl)-2-2-bipyridine)Cl; L_1H_3: Ir(3-(2-pyridyl)benzoic acid)$_3$; L_2H_3: Ir(4-(2-pyridyl)benzoic acid)$_3$ ppy: 2-phenylpyridine anion; NPh_2: diphenylamine; mebtp: 2-benzo[b]thiophene-2-yl-4-methyl-pyridine; MCM-41: mobil catalytic material 41; TEOS: tetraethyl orthosilicate; ORMOSIL: organically modified silicates; ALOOH: aluminium oxide/hydroxide; FIB: poly(1,1,1,3,3,3-hexafluoroisoproplylmethacrylate-co-1H,1H-dihydroperfluorobutyl-methacrylate).

Sanchez-Barragan et al. [27] and Borisov et al. [28] have summarized the luminescence probes used for analyzing oxygen). However, it is likely the determination of trace oxygen concentrations by means of the quenching of the luminescence is still being developed. Table 1 shows a summary about the most recent iridium and ruthenium dyes used for oxygen sensing, as a continuation of the previous table reported in Fernandez-Sanchez et al. [17].

In this paper, we propose four novel Iridium(III) complexes: bis(2,4-difluorophenylpyridine)-4,4′-tert-butyl-2,2′bypyridine iridium(III) hexafluorophosphate (called N969), 4,7-diphenyl-1,10-phenanthroline-bis(2phenylpyridine)iridium(III) hexafluorophosphate (called N1001), [Ir(2,4-difluorophenylpyridine)$_2$(4,7-diphenyl-1,10-phenanthroline)](PF_6) (called N1008) and [Ir(2-phenylpyridine)$_2$(4-bromo-2,2′-bipyridine)](PF_6) (called N1010) as oxygeNsensitive probe when they are immobilized in polymeric films (polystyrene with and without plasticizers) and aluminum oxide-hydroxide nanostructured solid support. The synthesis of the complexes N969 and N1001 have been previously published [39,40] but they have not been used as oxygen probe; this paper also shows the synthesis of complexes N1008 and N1010. These dyes were selected to cover a large variety of properties, such as a wide range of emission wavelengths which vary from 463 to 624 nm in solution, low to high quantum yield, and an expected high sensitivity to low oxygen concentrations, according to previous studies developed by our research group [17,19,21], which make them interesting not only for controlling residual oxygen or anaerobic conditions, but also in applications that requires different wavelengths and sensitivities.

2. Materials and methods

2.1. Materials

For the synthesis of the Ir(III) complexes, the following chemicals were used: $IrCl_3 \cdot xH_2O$ (Heraeus), 2-phenylpyridine (Sigma–Aldrich), 4,7-diphenylphenanthroline (Sigma–Aldrich). 2-(2,4-Difluorophenyl)pyridine was synthesized as reported in the literature [41].

For the preparation of the membranes, synthesized dyes were used as well as chloroform (Fluka), quinine sulphate (Fluka), polystyrene (Scientific Polymers, USA) and *o*-cyanophenyl octyl ether (from Fluka, puriss.). The gas flow-system was supplied by 50 L gas bottles at 200 bars with nitrogen 60 and oxygen 55 (both from Air Liquid, Spain).

2.2. Synthesis of Ir-complexes

[Ir(2,4-difluorophenylpyridine)$_2$-(4,4′-dimethylamino-2,2′-bipyridine)](PF_6) (N969) [39] and [Ir(2-phenylpyridine)$_2$(4,7-diphenyl-1,10-phenanthroline)](PF_6) (N1001) [40] were synthesized as described in the literature.

Based on the similar procedures, [Ir(2,4-difluorophenylpyridine)$_2$(4,7-diphenyl-1,10-phenanthroline)](PF_6) (N1008) and [Ir(2-phenylpyridine)$_2$(4-bromo-2,2′-bipyridine)](PF_6) (N1010) have been synthesized in a low boiling solvent, dichloromethane, by reaction of the corresponding dichloro-bridged iridium(III) dimer with 2.5 equivalents of 4,7-diphenyl-1,10-phenanthroline or 4-bromo-2,2′-bipyridine ligand, respectively.

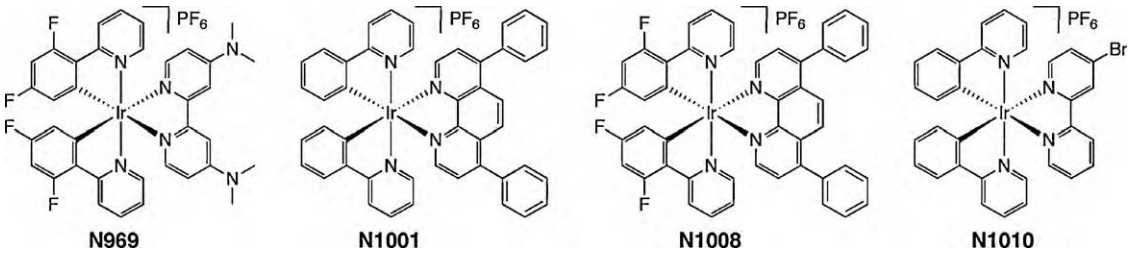

Fig. 1. Chemical structures of the Ir(III) complexes N969, N1001, N1008 and N1010.

Fig. 1 shows the chemical structures of the Ir(III) complexes and Electronic Supporting Information (ESI) shows the aromatic part of ^{1}H NMR spectrum of N1008 and N1010 in $CDCl_3$.

2.3. [Ir(2,4-difluorophenylpyridine)2(4,7-diphenyl-1,10-phenanthroline)](PF6) (N1008)

Yield: 132 mg, 68%. Anal. Calcd for $C_{46}H_{28}F_{10}IrN_4P$: C, 52.62; H, 2.69; N, 5.34. Found: C, 52.84; H, 2.53; N, 5.37. ^{1}H NMR ($CDCl_3$): *d* 8.34–8.29 (4H, m), 8.18 (2H, s), 7.79 (2H, dt, *J* = 4.0, 0.8 Hz), 7.75 (2H, d, *J* = 5.2 Hz), 7.66–7.49 (12H, m), 7.10 (2H, dt, *J* = 7.6, 2.0 Hz), 6.62 (2H, ddd, *J* = 12.4, 9.2, 2.4 Hz), 5.81 (2H, dd, *J* = 8.4, 2.0 Hz). ES-MS *m*/*z* (Calcd): 905.1668 (905.1879) $[M]^+$.

2.4. [Ir(2-phenylpyridine)$_2$(4-bromo-2,2′-bipyridine)](PF$_6$) (N1010)

Yield: 787 mg, 79%. Anal. Calcd for $C_{32}H_{23}BrF_6IrN_4P$: C, 43.64; H, 2.63; N, 6.36. Found: C, 43.79; H, 2.51; N, 6.37. ^{1}H NMR ($CDCl_3$): *d* 8.67 (1H, d, *J* = 1.6 Hz), 8.60 (1H, d, *J* = 8.4 Hz), 8.17 (1H, dt, *J* = 8.0, 1.6 Hz), 7.95–7.88 (3H, m), 7.77 (2H, dt, *J* = 8.4, 1.6 Hz), 7.73 (1H, d, *J* = 6.0 Hz), 7.68 (2H, ddd, *J* = 7.6, 2.8, 0.8 Hz), 7.59 (1H, d, *J* = 5.6 Hz), 7.53 (2H, m), 7.45 (1H, dt, *J* = 5.6, 1.2 Hz), 7.09 (2H, m), 7.03 (2H, tt, *J* = 7.6, 1.2 Hz), 6.91 (2H, dt, *J* = 7.6, 0.4 Hz), 6.27 (2H, ddd, *J* = 7.6, 4.4, 0.8 Hz). ES-MS *m*/*z* (Calcd): 735.0544 (735.0735) $[M]^+$.

2.5. Instrumentation

All luminescence measurements were carried out on a Varian Cary-Eclipse luminescence spectrometer equipped with a Xe flash lamp (peak power equivalent to 75 kW), Czerny-Turner monochromators, R-928 photomultiplier tube which is red sensitive (even 900 nm) with manual or automatic voltage.

For gas mixing, two mass-flow controllers (MFC) of Type EL-FLOW® model F-201CV Bronkhorst High-Tech (Ruurlo, Netherlands) were used. After the MFCs, copper and stainless steel tubing was used to connect the MFC with the self-built flow-through cell [19].

The system was controlled by Cary Eclipse software for Windows 95/98/NT which fully controls the luminescence spectrometer. The O_2-gas station was controlled by a self-written LabView 8.2 program connected to a Flow Bus interface (Bronkhosrt) that fully controls the Bronkhosrt mass-flow controllers via RS-232.

2.6. Preparation and characterization of oxygen sensing films

The nanostructured matrix was prepared by Ilford Imaging Switzerland following the procedure previously published [17,19–23]. The membrane used is called AP200/19 and it is based on aluminum oxide hydroxide coated by courting coating in PET, providing a positively charged nanostructured film with a pore diameter of 19 nm and a total pore volume of 20 mL/m^2.

Table 2
Nomenclature and composition of the oxygeNsensitive membranes. PS, polystyrene; *o*-CPOE, *o*-cyanophenyl octyl ether.

Name	wt.% PS	wt.% plasticizer	wt.% dye
PSOX	98.5	0	1.5
PS1X	90	8.5	1.5
PS2X	81	17.5	1.5

The cocktails were prepared in sealable 4 mL flasks and then were filled up to 2 mL solution volume with chloroform (dye concentration of 1.5 mg mL^{-1}). Table 2 shows the composition and the nomenclature of the different polystyrene cocktails, which were shaken on a Vortex-Genie® 2 (Scientific Industries, Bohemia, NY, USA) equipped with a home-made holder for multiple vials until all components were dissolved. The membranes were obtained using a Laurell spiNcoater model WS-400B-6NPP/LITE (North Wales, PA, USA). For polystyrene membranes, 200 μL of the cocktail was injected onto a rotating glass plate of a spinning device at 700 rpm. For the metal oxide, nanostructured membranes, 100 μL of the cocktail, containing only a solution of the dye, was injected onto the rotating metal oxide support fixed onto a spinning device at 300 rpm. Both, PS and AP200/19 membranes were transparent and allowed visible light to pass through. The resulting layers showed a thickness between 2 and 7 μm, depending on viscosity of the polymer mixture. Further optimization in thickness influence will have to be carried out for the corresponding application.

A standard protocol was used for characterizing the membranes. See Table 3 for the standard settings. A time trace curve (see Fig. 2a) was used to recorder I_0 and I.

To obtain the Stern–Volmer Plot (SVP), the oxygen partial pressures were calculated from the measured oxygen/nitrogen flows, assuming a constant environmental pressure of 1000 mbar. All the measurements were made at 10 different oxygen partial pressures between 0 and 0.1 bar and a room temperature of 21 °C (see Fig. 2).

In addition, three replicas for each kind of membrane were prepared in order to evaluate the error. The experimental results were expressed as the average of 3 replicas ± error ($s \cdot t/\sqrt{n}$), where s is the standard deviation, t the student t and n the number of replicas.

3. Results and discussion

3.1. Spectroscopic behavior of the oxygeNsensitive material

Full photophysical properties of the dyes N969 [39] and N1001 [40] have been previously described in the literature. UV–vis absorption spectra for the four dyes in acetonitrile solution at 298 K display strong bands in the UV due to intraligand π–π* transitions and smaller bands in the visible due to metal-to-ligand charge-transfer (MLCT). When excited in acetonitrile solution within the MLCT absorption band, N1008 and N1010 complexes show emission maxima at 538 and 624 nm, respectively, with luminescence quantum yield of 0.73 and 0.05, respectively (see Fig. 3). The tuning of the emission maximum in the new dyes can be rationalized by taking into account the donor–acceptor character of the sub-

Table 3
Maximum luminescence excitation and emission wavelengths, $\lambda_{exc/em}$, and luminescence quantum yield (Φ_{LX}) for the organometallic complexes dissolved in acetonitrile and incorporated into polystyrene (PS) and the metal oxide matrix AP200/19. ([dye] = 1.5 mg mL^{-1}; monochromator slit width$_{exc/em}$=20/20 nm).

Dye	Solution		Membrane	$\lambda_{ex}/\lambda_{em}$ (nm)	Detector voltage (V)	Φ_{LX}[a]
	$\lambda_{ex}/\lambda_{em}$ (nm)	Φ_{LX}				
N969	380/463	0.85	PSOX PS1X PS2X AP200/19	385/585 350/490	750 590	0.86±0.05
N1001	470/605	0.53	PSOX PS1X PS2X AP200/19	300/530 330/549	800 660	0.64 ± 0.05
N1008	400/538	0.73	PSOX PS1X PS2X AP200/19	305/510 340/512	550 	0.92 ± 0.05
N1010	450/624	0.05	PSOX PS1X PS2X AP200/19	300/520 330/545	770 	0.14 ± 0.05

[a] The luminescence quantum yields were calculated for the membrane PS0X according to reference 17 and the results are expressed as the average of three replicas $\pm st/\sqrt{n}$ (n = 3, t = 4.30 (2P = 0.05)).

stituents and their impact on the HOMO and LUMO energy levels, as it is understood for other iridium-complexes. [42] The blue shift of emission maximum observed in N1008 when compared to N1001 which has similar structure, is attributed to the addition of fluorine on the phenyl ring of the main ligand. Indeed, as in this type of complexes the HOMO orbital is mainly localized on this phenyl ring, the strong acceptor character of fluorine atoms stabilizes the HOMO energy level significantly more than the LUMO energy level, hence increasing the HOMO-LUMO gap. On the other hand, the red shift observed with N1010 when compared to the parent complex Ir(2-phenylpyridine)$_2$(bipyridine)$^+$ which emits at 585 in acetonitrile [43] is attributed to the bromine substituent on the bipyridine ancillary ligand. As the LUMO orbital is mainly localized on the ancillary ligand in this type of complex, the acceptor character of the bromine stabilizes the LUMO energy level much more than the HOMO energy level, hence decreasing the HOMO–LUMO gap. The observed photoluminescence quantum yields in solution is tentatively explained by the energy gap law which states that the noNradiative decay rate increases exponentially as the emission energy decreases. An increase of the noNradiative decay rate induces a decrease of the photoluminescence quantum yield which is observed when going in order of decreasing emission energy from N969 to N1008 to N1001 to N1010 which emit at 463, 538, 605 and 634 with photoluminescence quantum yields of 0.85, 0.73, 0.53 and 0.05, respectively.

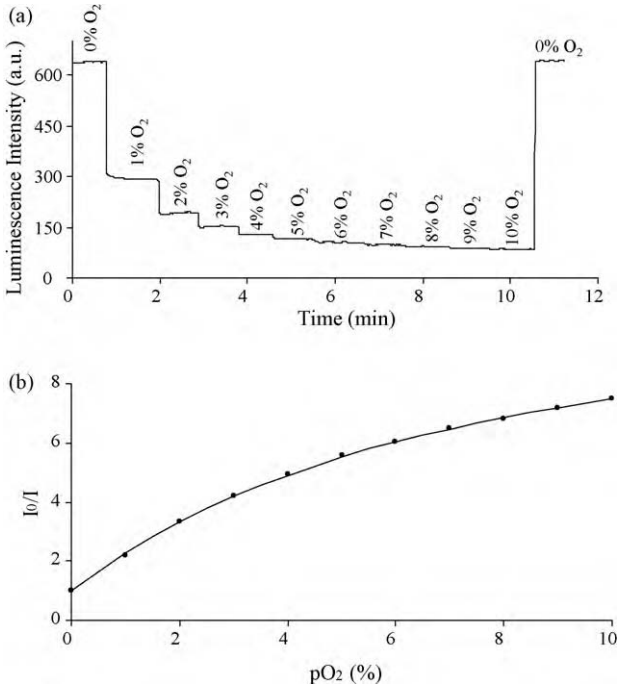

Fig. 2. (a) Example of time trace curve for the PS0X membrane of N1001. (b) Stern–Volmer plot obtained for this membrane adjusting the data by Lehrer; [N1001] = 1.5 mg mL^{-1}; $\lambda_{exc/em}$ = 305/510 nm; slit width$_{exc/em}$ = 20/20 nm, t_d = 120 μs and t_g = 5 ms.

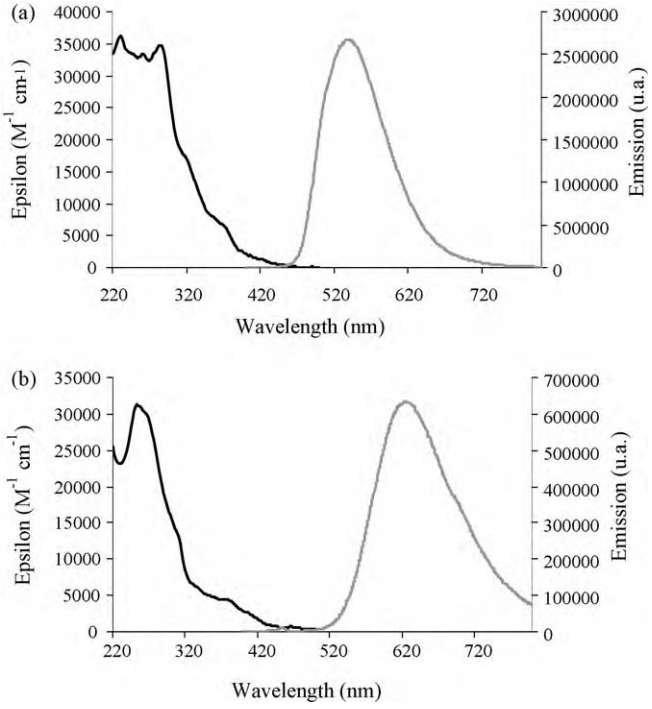

Fig. 3. Absorption (black line) and emission (grey line) spectra in acetonitrile for N1008 (a) and N1010 (b).

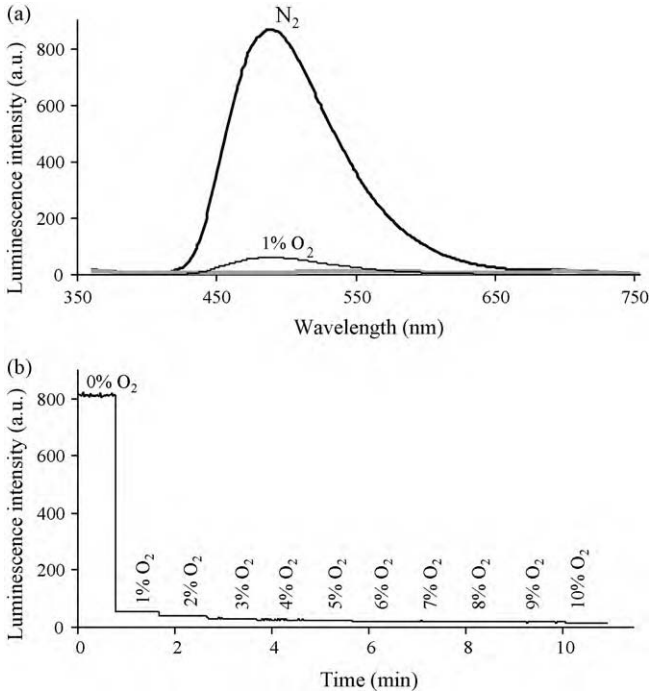

Fig. 4. (a) Emission spectra of N969 incorporated into AP200/19 when in absence of oxygen (bold, black line), in presence of 1% oxygen (thin, black line) and with 10% of oxygen (grey line); (b) relative luminescence intensity of N969 incorporated into AP200/19 at different concentration levels of O_2; [dye] = 1.5 mg mL^{-1}; λ_{exc} = 385 nm, monochromator slit width$_{exc/em}$ = 20/20 nm, t_d = 120 μs; t_g = 5 ms.

Table 2 shows the composition and the terminology of the different sensing films studied, and Table 3 shows the luminescence excitation and emission properties of the different sensing layers. In addition, Table 3 also shows the luminescence quantum yield of the four Ir-complexes in solution and incorporated into the solid support. The luminescence quantum yields of the thin films were calculated according with reference [17] selecting 0.2 mg/L of quinine sulfate in sulfuric acid as reference, assuming a luminescence quantum yield of 0.54 [44].

The incorporation of the dyes into a solid support generally increases the luminescence quantum yield compared to the solution. This is due to the more rigid environment in the solid support which decreases the noNradiative constant. A recent example shows this is very advantageous for iridium-complexes used in light-emitting devices [45].

For all the membranes, similar excitation and emission profiles were obtained (see Fig. 4a; Electronic Supporting Information (ESI) shows all the spectra for the four complexes immobilized in all the solid supports). For all of them, when molecular oxygen concentration is over 10%, the luminescence is completely quenched.

The different composition of the matrix has different impact on the aggregation behavior of the different dyes depending on their chemical structure. This hypothesis is further supported by the need of a two-site model most of the case (*vide infra*), which already requires dyes with at least two different environment, but not for N1008 in the present work. Furthermore, the different emission maxima observed in matrices can be in general explained by an expected difference in polarity of the medium. It is commonly known that emission maxima depends on polarity of the surrounding because in those complexes, emission is usually coming from charge-transfer (CT) excited state [46] which energy level can be destabilized in noNpolar solvents (blue shift) and stabilized in polar solvents (red shift) in the case where the CT state has a higher dipole moment than the ground state. While it is expected that for the present complexes the emission is coming from a ^{3}MLCT state involving the ancillary bipyridine, further explanation requires quantitative knowledge about the type of CT state involved in the emission, implying the need for quantum chemical calculations which is out of the scope of the present paper. In all the cases the lifetime was lower than 50 μs; thus, it was not possible to measure the luminescence lifetime of the oxygeNsensitive membranes because the available instrumentation does not provide reliable data when the lifetime is lower than 50 μs.

3.2. Oxygen sensitive properties

Luminescence quenching methods of analysis are based on the decrease in emission intensity in the presence of the quencher (oxygen), and are described by the Stern–Volmer equation (see Eq. (1)) [14,17,19,21,25].

$$\frac{I_0}{I} = 1 + k_{SV} pO_2 \quad (1)$$

where I is the luminescence intensity, the subscript "0" refers to the value in the absence of quencher, k_{SV} is the Stern–Volmer constants and pO_2 is the partial pressure of oxygen. However, deviations have been observed, and these are often attributed to the heterogeneity of the media in which the dye is dispersed. In fact, only one of the dyes, N1008, shows a linear SV plot when it is dissolved in PS with and without plasticizer.

The heterogeneity is attributed to different types of oxygen quenching sites within the matrix [17,19,21]. Therefore, this curvature of the Stern–Volmer plot needs a more complex model to be explained. In this case we obtained that the minimal model necessary to fit the experimental data was a two-site model. One of these models was proposed by Demas and co-workers, so-called the Demas' model [47] (see Eq. (2)):

$$\frac{I_0}{I} = \left[\frac{f_1}{1 + k_{SV,1} pO_2} + \frac{f_2}{1 + k_{SV,2} pO_2}\right]^{-1} \quad (2)$$

where f_i denotes the fractional contribution of the total luminescence emission from the luminophore located at site type i under unquenched conditions, which exhibit a discrete Stern–Volmer quenching constant given by k_{SVi}. Other two-site model was proposed by Lehrer [48] in which only one microenvironment is accessible to the quencher ($k_{SV,2} = 0$; see Eq. (3))

$$\frac{I_0}{I} = \left[\frac{f_0}{1 + k_{SV} pO_2} + (1 - f_0)\right]^{-1} \quad (3)$$

where f_0 denotes the fraction of the total luminophore's population that is accessible to the quencher, and k_{SV} is the Stern–Volmer quenching constant which is associated with the accessible fraction of luminophores.

Practically in all the cases, except for the dye N1008 incorporated into PS, the experimental results cannot be explained by a linear relationship, thus a two-site model has to be used to fit the experimental data (see Fig. 2). In addition, the fitting of the experimental data by using the Demas' model provides incorrect results; only Lehrer's model may be used to fit the experimental data. It means that the oxygeNsensitive nanostructured membranes are heterogenic which could explain the experimental results on AP200/19: the dye is located in two different environments, one which can be quenched by oxygen and another where oxygen is not able to quench it or has not access. Similar results with similar kind of complexes have been previously reported [17,19,21]. Another explanation could be based on dye aggregation effects which are more frequent on polymer films, providing similar results that when using nanostructured metal oxides. These hypotheses could explain why the Lehrer's model fits the experimental data.

Table 4
Oxygen sensitivity and $\Delta I_{1\%}$ of iridium(III) complexes incorporated into the AP200/19 and PS films ([dye] = 1.5 mg mL^{-1}; slit width$_{exc/em}$ = 20/20 nm; t_d = 120 μs; t_g = 5 ms; for $\lambda_{exc/em}$ see Table 2).

Dye	Membrane	Lehrer's model[a]		$\Delta I_{1\%}$[a] (%)	$p_{O_2}(S = 1/2)$
		k_{SV} (bar^{-1})	f_0		
N969	PSOX	358 ± 24	0.81 ± 0.02	79.66 ± 2.34	0.0045
	PS1X	87 ± 2	0.82 ± 0.01	52.32 ± 0.58	0.0180
	PS2X	53 ± 2[b]	1	41.63 ± 1.31	0.0189
	AP200/19	1231 ± 150	0.99 ± 0.00	93.13 ± 0.13	0.0008
N1001	PSOX	164 ± 11	0.92 ± 0.01	55.29 ± 2.40	0.0073
	PS1X	196 ± 32	0.95 ± 0.00	59.31 ± 8.34	0.0057
	PS2X	96 ± 11	0.97 ± 0.00	46.96 ± 2.62	0.0111
	AP200/19	2848 ± 101	0.78 ± 0.06	76.05 ± 5.73	0.0006
N1008	PSOX	72 ± 5[b]	1	40.96 ± 2.29	0.0139
	PS1X	34 ± 1[b]	1	27.48 ± 0.39	0.0294
	PS2X	28 ± 6[b]	1	25.46 ± 2.95	0.0357
	AP200/19	222 ± 8	0.96 ± 0.00	73.52 ± 2.54	0.0049
N1010	PSOX	313 ± 23	0.51 ± 0.03	38.97 ± 2.06	0.1597
	PS1X	103 ± 1	0.91 ± 0.00	54.35 ± 1.57	0.0118
	PS2X	113 ± 0	0.80 ± 0.10	48.05 ± 3.08	0.0147
	AP200/19	561 ± 112	0.21 ± 0.13	14.50 ± 2.82	−0.0031

[a] The experimental results have been expressed as the average of 3 replicas $\pm s \cdot t/\sqrt{n}$ (n = 3, t = 4.30 (2P = 0.05)).
[b] Values obtained by a linear fitting.

Table 4 shows the k_{SV} for all the membranes. The analysis of the experimental results shows that the highest Stern–Volmer constant, k_{SV} equal to 2848 ± 101 bar^{-1}, corresponds to N1001 incorporated into AP200/19. In general, the incorporation of the dyes into AP200/19 provides higher k_{SV} than within the PS-matrix. This effect of the AP200/19 matrix may rather be traced back to the capillary forces and the permeation of oxygen through the nanostructured matrix than to the chemical environment of the pores. The metal oxide matrix is formed from agglomerated particles, where the nanopores are located inside while the macropores appear between agglomerated particles [22]. Since the capillary forces are high, the oxygen is quickly driven into the nanopores (pore diameter = 19 nm) [22]. This structure was shown before to be responsible for the much higher sensitivity of different OMCs, Ru(II)- as well as a variety of iridium-complexes (N926, N833 and N837), to oxygen compared to the polystyrene matrix [21].

The results in Table 4 also show that using the plasticizer (*o*-CPOE) decreases the k_{SV}. Medina-Castillo et al. have previously demonstrated that *o*-CPOE quenches the luminescence emission of the metal complex and thus reduces the fraction of the luminescent dye that is accessible for luminescence quenching by oxygen [19].

Table 4 also shows the parameters $\Delta I_{1\%}$ and $p_{O_2}(S = 1/2)$ as rough guides to the sensitivity of the optical oxygen sensing films.

$p_{O_2}(S = 1/2)$ is defined as the value of the partial pressure of oxygen necessary to reduce the initial (oxygen free) luminescence exhibited by the film by 50%. From Eq. (3) it follows that:

$$p_{O_2}(S = 1/2) = \frac{1}{k_{SV}(2f_0 - 1)} \quad (4)$$

Table 4 shows that the incorporation of complexes into the nanostructured material provide lower $p_{O_2}(S = 1/2)$ than when the same dyes are immobilized into PS (except for the dye N1010); it means that the use of AP200/19 as solid support provide an increase on sensitivity. In addition, the lowest value of $p_{O_2}(S = 1/2)$ is obtained by N1001 immobilized in AP200/19 (0.0006). Therefore, it is possible to conclude that the most sensitive membrane consists on N1001 immobilized on the metal oxide, nanostructured support, corroborating the conclusion carried out by analyzing the values of the Stern–Volmer constants.

$\Delta I_{1\%}$ is defined as the percentage of the luminescence quenched at 1% oxygen and it was calculated according to equation 5:

$$\Delta I_{1\%} = \frac{I_0 - I_1}{I_0} \times 100 \quad (5)$$

where $\Delta I_{1\%}$ is the percentage of luminescence quenched at 1% of oxygen, I_0 corresponds to the intensity of the film in absence of oxygen and I_1 is the intensity in the presence of a 0.01 bar (1%) of oxygen. Since the available instrumentation was not able to create flows below 1% O_2, the parameter $\Delta I_{1\%}$, were chosen to evaluate which membranes are expected to be more appropriate to be used for oxygen concentrations between 0 and 1%. This shows the ability of each sensing film to be used in applications that require the control of very low concentration of molecular oxygen, such as intelligent packaging or control of inert atmospheres, among others, although a deep study of sensitivity between 0 and 1% of oxygen should be carried out in further studies.

As can be seen in Table 4, the incorporation of complexes into the nanostructured material provide higher $\Delta I_{1\%}$ than when the same dyes are immobilized into PS (except for the dye N1010); similar to $p_{O_2}(S = 1/2)$. In fact, the oxygen sensing film that show higher $\Delta I_{1\%}$, and therefore may be the most suitable for the uses mentioned above, is prepared by the incorporation of the dye N969 into AP200/19 (see Fig. 4). It shows a $\Delta I_{1\%}$ value of 93.13 ± 0.13%. It can be also seen that, in general the addition of plasticizer to the cocktail composition decreases the $\Delta I_{1\%}$.

3.3. Reversibility, response time and long-term stability

Fig. 2a shows the luminescence intensity of N1001 membrane which varies with the partial pressure of oxygen. The complete reversibility of the luminescence emission of the oxygeNsensitive films allows to monitor an increasing and decreasing pO_2 continuously. The physico-chemical quenching reaction is a reversible process.

In addition, the oxygeNsensitive membranes show quick response times: the t_{95} response time for all of the studied sensing films were lower than 2 s when changing from 0 vol.% pO_2 to 1 vol.% pO_2, and lower than 4 s when changing from 10 vol.% pO_2 to 0 vol.% pO_2.

Since their analytical performance (k_{SV}) did not change over 1 year storage under ambient conditions, the long-term stabil-

ity of all the oxygeNsensitive membranes might be considered to be sufficiently good for measurements in the gas phase (see ESI). Furthermore, after excitation during 24 h at the corresponding excitation wavelength, the sensitivity did not change, so the photochemical stability seems to be good for any further applications (see ESI).

4. Conclusions

The luminescent iridium-complexes N969, N1001, N1008 and N1010 were investigated in view of their application in oxygeNsensitive chemical sensors. The organometallic complexes were incorporated into a nanostructured metal oxide matrix as well as into a solvent polymeric polystyrene membrane and characterized in the gas phase for its response to oxygen. The films show one emission band which is quenched for oxygen concentrations over 10%.

The luminescence quantum yields were determined, resulting in a very high value for the dyes N969 and N1008. The most sensitive films is based on the dye N1001 incorporated into AP200/19, showing a Stern–Volmer constant equal to 2848 ± 101 bar^{-1} and a $p_{O_2}(S = 1/2)$ equal to 0.0006. In addition, the parameter $\Delta I_{1\%}$ was evaluated in order to establish the most sensitive sensing films for controlling very low concentrations (lower than 1%) of molecular oxygen. In this case, the most sensitive film was the N969 incorporated into AP200/19, with $\Delta I_{1\%}$ value of 93.13 ± 0.13%, which is between 1.5 and 6 times higher than in other films.

An overview of luminescence probes used for analyzing oxygen shows that the dyes characterized in this work provide higher sensitivity, even for lower oxygen concentration, than the previously reported in the literature. When comparing these dyes with N833, N837, N926 [17] and N948 [19] supported into PS, it can be noticed than for similar quantum yields, in most of the membranes, the values of the Stern–Volmer constants are over 100 times higher; even when comparing these dyes into the nanostructured support [19,20], for a 10 times lower oxygen concentrations, values of k_{SV} are between 10 and 100 times higher. Unfortunately, no satisfying trend can be observed at the moment between sensing performances of the films and properties of the dyes in solution, which would be of great help for designing further improved sensing dyes. A first reason is due to the different photophysical properties of dyes in solution compared to dyes in a solid matrix. Second, it is likely that the composition of the matrix has an impact on the aggregation behavior of the dyes. The observed oxygen sensing performances are the result of an interplay between intrinsic dyes performances, dyes aggregation behavior and film morphology. Conclusions can be made only on the films performances as a whole, not on a single factor.

Finally, the transparent oxygeNsensitive films show complete reversibility with short response times and very long-term stability, higher than 1 year.

Acknowledgments

The authors gratefully acknowledge the financial support of the Junta de Andalucía (Excellence Project FQM-02625 and MaríN-SuárezdelToro's grant). Also, the authors are grateful to Ilford Imaging Switzerland GmbH (Switzerland) for supplying the metal oxide membranes and Dr. de la Torre-Vega and Ing. Rodriguez-Medina for automating the O_2-gas station.

Appendix A. Supplementary data

Supplementary data associated with this article can be found, in the online version, at doi:10.1016/j.talanta.2010.05.018.

References

[1] E.W. Stein, P.S. Grant, H. Zhu, M.J. McShane, Anal. Chem. 79 (2007) 1339–1348.
[2] E.J. Park, K.R. Reid, W. Tang, R.T. Kennedy, R. Kopelman, J. Mater. Chem. 15 (2005) 2913–2919.
[3] W.L. Rumsey, J.M. Vanderkooi, D.F. Wilson, Science 241 (1988) 1649–1651.
[4] F.C. O'Mahony, T.C. O'Riordan, N. Papkovskaia, V.I. Ogurtsov, J.P. Kerry, D.B. Papkovsky, Packag. Technol. Sci. 14 (2004) 225–234.
[5] A. Mills, Chem. Soc. Rev. 34 (2005) 1003–1011.
[6] T.C. O'Riordan, H. Voraberger, J.P. Kerry, D.B. Papkovsky, Anal. Chim. Acta 530 (2005) 135–141.
[7] F.A. Rainey, A. Oren, in: F.A. Rainey, A. Oren (Eds.), Extremophiles, Academic Press, Amsterdam, 2006.
[8] R.C. Soliva-Fortuny, O. MartíNBelloso, Trends Food Sci. Technol. 14 (2003) 341–353.
[9] K. Palmer-Wright, A.A. Kader, Postharvest Biol. Technol. 10 (1997) 89–97.
[10] S.C. Fonseca, F.A.R. Oliveira, J.K. Brecht, K.V. Chau, Postharvest Biol. Technol. 35 (2005) 279–292.
[11] E. Vilas-Boas, A.A. Kader, Postharvest Biol. Technol. 39 (2006) 155–162.
[12] J.R. Gorny, B. Hess-Pierce, R.A. Cifuente, A.A. Kader, Postharvest Biol. Technol. 24 (2002) 271–278.
[13] F. Carlin, C. NguyeNThe, Y. Chambroy, M. Reich, Int. J. Food Sci. Technol. 25 (1990) 110–119.
[14] G. Orellana, Anal. Bioanal. Chem. 379 (2004) 344–346.
[15] A.S. Kocincova, S.M. Borisov, C. Krause, O.S. Wolfbeis, Anal. Chem. 79 (2007) 8486–8493.
[16] A. Hakonen, S. Hulth, Anal. Chim. Acta 606 (2008) 63–71.
[17] J.F. Fernandez-Sanchez, T. Roth, R. Cannas, Md.K. Nazeeruddin, S. Spichiger, M. Graetzel, U.E. Spichiger-Keller, Talanta 71 (2007) 242–250.
[18] O.S. Wolfbeis, J. Mater. Chem. 15 (2005) 2657–2669.
[19] A.L. Medina-Castillo, J.F. Fernandez-Sanchez, C. Klein, Md.K. Nazeeruddin, A. Segura-Carretero, A. Fernandez-Gutierrez, M. Graetzel, U.E. Spichiger-Keller, Analyst 132 (2007) 929–936.
[20] J.F. Fernandez-Sanchez, T. Nezel, R. Steiger, U.E. Spichiger-Keller, Sens. Actuators B: Chem. 113 (2006) 630–638.
[21] J.F. Fernandez-Sanchez, R. Cannas, S. Spichiger, R. Steiger, U.E. Spichiger-Keller, Anal. Chim. Acta 566 (2006) 271–282.
[22] R. Steiger, R. Beer, J.F. Fernandez-Sanchez, U.E. Spichiger-Keller, Solid State Phenom. 121–123 (2007) 1193–1197.
[23] J.F. Fernandez-Sanchez, I. Fernandez, R. Steiger, R. Beer, R. Cannas, U.E. Spichiger-Keller, Adv. Funct. Mater. 17 (2007) 1188–1198.
[24] A. Gomez-Henz, M.P. Aguilar-Caballos, Trends Anal. Chem. 23 (2004) 127–136.
[25] G. Orellana, D. García-Fresnedillo, in: R. Narayanaswamy, O.S. Wolfbeis (Eds.), Optical Sensors, Springer, Berlin/Heidelberg, Germany, 2004, pp. 309–357.
[26] J.M. Costa-Fernández, A. Sanz-Medel, in: A. Fernandez Gutierrez, S.G. Schulman (Eds.), Analytical Molecular Fluorescence: A Practical Approach, Editorial Universidad de Granada, Granada, Spain, 2001, pp. 355–395 (in Spanish language).
[27] I. Sanchez-Barragan, J.M. Costa-Fernandez, M. Valledor, J.C. Campo, A. Sanz-Medel, Trends Anal. Chem. 25 (2006) 958–967.
[28] S.M. Borisov, I. Klimant, Anal. Chem. 79 (19) (2007) 7501–7509.
[29] X. Wu, L. Song, B. Li, Y. Liu, J. Lumin. 130 (2010) 374–379, 3.
[30] B.W.K. Chu, V.W.W. Yam, Langmuir 22 (2006) 7437.
[31] B. Lei, B. Li, H. Zhang, S. Lu, Z. Zheng, W. Li, Y. Wang, Adv. Funct. Mater. 16 (14) (2006) 1883–1891.
[32] H. Zhang, B. Li, B. Lei, W. Li, J. Lumin. 128 (2008) 1331–1338.
[33] H.J. Kim, Y.C. Jeong, J.I. Rhee, Talanta 76 (5) (2008) 1070–1076.
[34] X. Wu, Y. Cong, Y. Liu, J. Ying, B. Li, J. Sol–Gel Sci. Technol. 49 (3) (2009) 355–363.
[35] S.J. Payne, G.L. Fiore, C.L. Fraser, J.N. Demas, Anal. Chem. 82 (3) (2010) 917–921.
[36] Z. Xie, L. Ma, K.E. DeKrafft, A. Jin, W. Lin, J. Am. Chem. Soc. 132 (3) (2009) 922–923.
[37] C.S.K. Mak, D. Penflehner, M. Stich, O.S. Wolfbeis, W.K. Chan, H. Yersin, Chem. Mater. 21 (11) (2009) 2173–2175.
[38] B. Carlson, B.E. Eichinger, W. Kaminsky, G.D. Phelan, Sens. Actuators B: Chem. 145 (1) (2010) 278–284.
[39] F. De Angelis, S. Fantacci, N. Evans, C. Klein, S.M. Zakeeruddin, J.E. Moser, K. Kalyanasundaram, H.J. Bolink, M. Graetzel, M.K. Nazeeruddin, Inorg. Chem. 46 (2007) 5989–6001.
[40] H.J. Bolink, L. Cappelli, E. Coronado, M. Graetzel, E. Orti, R.D. Costa, P.M. Viruela, M.K. Nazeeruddin, J. Am. Chem. Soc. 128 (2006) 14786–14787.
[41] O. Lohse, P. Thevenin, E. Waldvogel, Synlett 1 (1999) 45–48.
[42] E. Baranoff, J.-H. Yum, M. Graetzel, M.K. Nazeeruddin, J. Organomet. Chem. 694 (17) (2009) 2661–2670.
[43] R.D. Costa, E. Orti, H.J. Bolink, S. Graber, S. Schaffner, M. Neuburger, C.E. Housecroft, E.C. Constable, Adv. Funct. Mater. 19 (2009) 3456–3463.
[44] W.H. Melhuish, J. Phys. Chem. 65 (1961) 229–235.
[45] E. Baranoff, S. Suarez, P. Bugnon, H.J. Bolink, C. Klein, R. Scopelliti, L. Zuppiroli, M. Grätzel, M.K. Nazeeruddin, Chemsuschem 2 (2009) 305–308.
[46] L. Flamigni, A. Barbieri, C. Sabatini, B. Ventura, F. Barigelletti, Top. Curr. Chem. 281 (2007) 143–203.
[47] J.N. Demas, B.A. DeGraff, Sens. Actuators B 11 (1991) 35–41.
[48] S.S. Lehrer, Biochemistry 10 (1971) 3254–3263.